EBERHARD KARLS UNIVERSITÄT TÜBINGEN
&
UNIVERSIDAD DE GRANADA

MASTER THESIS

Master thesis

Author:
Leopold BODAMER

Supervisor:
Prof. Dr. Daniel Manzano
Diosdado

A thesis submitted in fulfillment of the requirements
for the degree of Master of Science

in

Theoretical Atomic Physics and Synthetic Quantum Systems
Institut für Theoretische Physik

June 6, 2025

Contents

EBERHARD KARLS UNIVERSITÄT TÜBINGEN

Abstract

Mathematisch-Naturwissenschaftliche Fakultät
Institut für Theoretische Physik

Master of Science

Master thesis

by Leopold BODAMER

This thesis investigates the directional routing of excitations in atomic systems using subradiant states. Building on Bottarelli's quantum router , this thesis adapts the model to atomic systems, addressing the challenges of controlling interactions in fully connected systems. Atom light interactions have been heavily studied for atomic lattices . In this thesis three chains, that are connected by an equilateral triangle and an isosceles triangle are studied. By allowing different dipole orientations on each chain, three distinct topologies are considered. The results show that controlling the topology and the initial state enables directional routing, where a topology with equilateral triangle and aligned dipoles emerges as the most practical for stable readout.

Chapter 1

Introduction

1.1   Coherence and Excitation Transport

In this chapter, we aim to explain the phenomena of long coherences (lifetimes) and the excitation transport of light on a microtubule. The proposed model takes the following approach:

- The microtubule is modeled as a cylindrical structure consisting of nodes. Each node represents an atom, which is modeled as a two-level system. The number of atoms, N_{atoms}, is determined by the number of chains (n_{chains}) and the number of rings (n_{rings}), assuming fixed positions for these nodes.

- The system is restricted to a single excitation.

- A time-dependent coupling to an electric field is proposed, which may be either classical or quantum in nature. This coupling is intended to facilitate spectroscopy.

- Two types of Lindblad operators are introduced to model dissipation processes. Specifically:

    1. Spontaneous decay
    2. Dephasing

The Lindblad operators introduced to model the spontaneous decay and dephasing processes for each individual atom are defined as follows:

$$C_{\text{decay}}^{(i)} = \sqrt{\gamma_0}\,\sigma_-^{(i)}, \tag{1.1}$$

$$C_{\text{dephase}}^{(i)} = \sqrt{\gamma_\phi}\,\sigma_z^{(i)}, \tag{1.2}$$

where:

- $C_{\text{decay}}^{(i)}$ describes the spontaneous decay of the i-th atom, with a rate given by γ_0.

- $C_{\text{dephase}}^{(i)}$ describes the dephasing of the i-th atom, with a rate given by γ_ϕ.

- $\sigma_-^{(i)}$ is the lowering operator for the i-th atom, and $\sigma_z^{(i)}$ is the Pauli z-operator for the i-th atom.

1.2   Motivation

It is widely assumed that one of the crucial tasks currently facing quantum theorists is to understand and characterize the behaviour of realistic quantum systems. In any experiment, a quantum system is subject to noise and decoherence due to the unavoidable interaction with its surroundings. The theory of open quantum systems aims at developing a general framework to analyze the dynamical behaviour of systems that, as a result of their coupling with environmental degrees of freedom, will no longer evolve unitarily. [1]

2DES> [2], [3], [4]

NONlinear Optics> [5], [6]

Spectroscopy investigates the interaction between matter and electromagnetic radiation, offering a means to analyze composition and structure. Central to this analysis is the understanding of how molecules respond to specific frequencies of light, revealing information about their energy levels and bonding. Key concepts include wavelength (λ), wavenumber ($\bar{\nu}$), and frequency (ν). Wavelength, the distance between successive wave crests, is typically measured in nanometers or micrometers. Wavenumber, expressed in inverse centimeters (cm^{-1}), represents the number of waves per unit distance and is directly proportional to energy, defined as $\bar{\nu} = 1/\lambda$ (where λ is in cm). Frequency, the number of wave cycles per second, is measured in Hertz (Hz), and the angular frequency (ω) is related to frequency by $\omega = 2\pi\nu$. The relationship between angular frequency and wavenumber is given by $\omega = 2\pi c\bar{\nu}$, where c is the speed of light.

Next, I converted all units into femtoseconds (fs^{-1}), which is commonly used in time-domain spectroscopy.

Spectrometers are instruments designed to measure the intensity of light as a function of wavelength or frequency.

Different types of spectrometers are employed for various regions of the electromagnetic spectrum. Notably, UV-Vis spectrometers analyze absorption and transmission of ultraviolet and visible light, while infrared (IR) spectrometers measure the absorption of infrared light, providing insights into molecular vibrations. Nuclear Magnetic Resonance (NMR) spectrometers probe the magnetic properties of atomic nuclei, revealing molecular structure.

Chapter 2

Derivation of the Redfield Equation

The following derivation is part of [7]

2.1 Derivation from microscopic dynamics

The most common derivation of the Redfield master equation is based on open quantum theory. We will begin by discussing the general problem, where a small quantum system interacts with a larger environment. The total system Hilbert space $\mathcal{H}_T$ is divided into our system of interest, belonging to a Hilbert space $\mathcal{H}_S$, and the environment living in $\mathcal{H}_E$.

$$\mathcal{H}_T = \mathcal{H}_S \otimes \mathcal{H}_E. \tag{2.1}$$

The Redfield equation is then an effective motion equation for a this subsystem of interest S. The derivation can be found in several textbooks such as Breuer and Petruccione [8].

The evolution of the total system is given by the Liouville-Von Neumann equation, which represents the starting point of our derivation:

$$\dot{\rho}_T(t) = -i[H_T, \rho_T(t)], \tag{2.2}$$

where $\rho_T(t)$ is the density matrix of the total system, and H_T is the total Hamiltonian. Note that we used units where $\hbar = 1$. This equation can not be solved for arbitrary large enviroments. But as we are interested in the dynamics of the system without the environment, we trace over the environment degrees of freedom to obtain the reduced density matrix of the system $\rho(t) = \text{Tr}_E[\rho_T]$.

The total Hamiltonian can be separated as:

$$H_T = H_S \otimes \mathbb{1}_E + \mathbb{1}_S \otimes H_E + \alpha H_I, \tag{2.3}$$

where $H_S \in \mathcal{H}_S$, $H_E \in \mathcal{H}_E$, and $H_I \in \mathcal{H}_T$. H_I represents the interaction between the system and the environment with coupling strength α. The interaction term is typically decomposed as:

$$H_I = \sum_i S_i \otimes E_i, \tag{2.4}$$

where $S_i \in \mathcal{B}(\mathcal{H}_S)$ and $E_i \in \mathcal{B}(\mathcal{H}_E)$ are operators, that only act on the system and environment respectively.

The following requirements are to be fuildilled by the final derived Redfield equation:

- The equation should be linear in the system density matrix $\dot{\rho}_S(t) = F(\rho_S(t))$ (reduced equation of motion).

- The equation should be Markovian, meaning that the evolution of the system density matrix at time t only depends on the state of the system at time t and not on its past history $\dot{\rho}_S(t) = \rho_S(t)$.

- The equation should be trace-preserving, meaning that $\text{Tr}[\rho_S(t)] = \text{Tr}[\rho_S(0)]$ for all times t.

Unlike the Linblad equation it does not guarantee the complete (not even normal) positivity of the density matrix, which is a requirement for a physical state. So care has to be taken, when the Redfieldequation is useful. The equation will be valid in the weak coupling limit, meaning that the constant in the interaction Hamiltonian H_I fulfills $\alpha \ll 1$.

2.1.1   Interaction Picture

To describe the system dynamics, we move to the interaction picture where the operators evolve with respect to $H_S + H_E$. Any arbitrary operator O in the Schrödinger picture takes the form

$$\hat{O}(t) = e^{i(H_S + H_E)t} O e^{-i(H_S + H_E)t}, \tag{2.5}$$

in the interaction picture, and depends on time. States now evolve only according to the interaction Hamiltonian H_I, and the Liouville-Von Neumann equation (Eq. (2.2)) changes to:

$$\dot{\hat{\rho}}_T(t) = -i\alpha[\hat{H}_I(t), \hat{\rho}_T(t)], \tag{2.6}$$

which can be formally integrated as:

$$\hat{\rho}_T(t) = \hat{\rho}_T(0) - i\alpha \int_0^t ds [\hat{H}_I(s), \hat{\rho}_T(s)]. \tag{2.7}$$

This equation will be inserted in Eq. (2.6):

$$\dot{\hat{\rho}}_T(t) = -i\alpha \left[\hat{H}_I(t), \hat{\rho}_T(0)\right] - \alpha^2 \int_0^t \left[\hat{H}_I(t), \left[\hat{H}_I(s), \hat{\rho}_T(s)\right]\right] ds, \tag{2.8}$$

which is not Morkovian, because of the intergal which sums up all the past. The step of integration and insertion can be repreated leading to a series expansion of the density matrix in the small parameter α:

$$\dot{\hat{\rho}}_T(t) = -i\alpha \underbrace{\left[\hat{H}_I(t), \hat{\rho}_T(0)\right]}_{(1)} - \alpha^2 \int_0^t \underbrace{\left[\hat{H}_I(t), \left[\hat{H}_I(s), \hat{\rho}_T(t)\right]\right]}_{(2)} ds + \mathcal{O}(\alpha^3). \tag{2.9}$$

where third order contributions (and higher) are neglected from now on. This can be justified in the weak coupling limit where $\alpha \ll 1$, which represents the "**Born**" approximation.

In this sense, the Redfield equation will be a second-order approximation of the actual dynamics. The weak coupling assumption does not hold universally and cannot be applied to all systems. For instance, it is often invalid in chemical or biological systems.

Remark, that Eq. (2.9) is still not Morkovian, because of the intergal over time. Since we are only interested in the dynamics of the system S, we will now take the partial trace over the environment degrees of freedom in Eq. (2.9).

2.1.2   Partial Trace

We now assume the whole system to be seperatable at $t = 0$ as a product state:

$$\hat{\rho}_T(0) = \hat{\rho}_S(0) \otimes \hat{\rho}_E(0), \tag{2.10}$$

which means, that the two sub-systems only come into contact at $t = 0$ and there are no correlations. We take the interaction Hamiltonian Eq. (2.4), which has the same shape in the Interaction Picture into account. With this, the partial trace over the environment of the part (1) of Eq. (2.9) is given by:

$$\sum_i \text{Tr}_E\big[S_i \otimes E_i, \hat{\rho}_S(0) \otimes \hat{\rho}_E(0)\big] = \sum_i \big(S_i\hat{\rho}_S(0) - \hat{\rho}_S(0)S_i\big) \cdot \text{Tr}_E\big[E_i\hat{\rho}_E(0)\big], \tag{2.11}$$

where we used the cyclic property of the trace. We define the average of the bath degrees of freedom at zero temperature:

$$\langle E_i \rangle_0 \equiv \text{Tr}_E\big[E_i\hat{\rho}_E(0)\big]. \tag{2.12}$$

which results to zero, simplifying Eq. (2.9) to only the second part. This can always be justified when adding a zero to the total Hamiltonian:

$$H_T = H_S' + H_E + \alpha H_I', \tag{2.13}$$

where a new interaction and system Hamiltonian are introduced. The interaction Hamiltonian takes new environmental operators E_i' which are shifted by the average of the environment operators at time $t = 0$:

$$H_I' = \sum_i S_i \otimes E_i' = \sum_i S_i \otimes (E_i - \langle E_i \rangle_0). \tag{2.14}$$

The new system Hamiltonian is then given by the sum of the original system Hamiltonian shifted proportionally by the average of the environment operators at time $t = 0$:

$$H_S' = H_S + \alpha \sum_i S_i \langle E_i \rangle_0, \tag{2.15}$$

This however doesn't change the structure of the system dynamics. It only accounts for a redefinition of the energy levels ("a sort of renormalization"). This way the equation (2.11) results to zero and only the second part of the equation Eq. (2.9) remains.

$$\dot{\rho}_S(t) = -i\alpha[\hat{H}_I(t), \hat{\rho}_T(0)] - \alpha^2 \int_0^t ds \text{Tr}_E\big[\hat{H}_I(t), [\hat{H}_I(s), \rho_S(t) \otimes \rho_E]\big]$$
$$= -\alpha^2 \int_0^t ds \text{Tr}_E\big[\hat{H}_I(t), [\hat{H}_I(s), \rho_S(t) \otimes \rho_E]\big]. \tag{2.16}$$

In the follwoing, we will derive the final expression by calculating the environmental traces in the last equation.

2.1.3   Final Expression

Defining $s' = t - s$, we rewrite the second-order term as:

$$\dot{\rho}_S(t) = \alpha^2 \int_0^t ds \, \text{Tr}_E \Big\{ \hat{H}_I(t) \big[\hat{H}_I(t - s)\hat{\rho}_T(t) - \hat{\rho}_T(t)\hat{H}_I(t - s) \big]$$

$$- \big[\hat{H}_I(t - s)\hat{\rho}_T(t) - \hat{\rho}_T(t)\hat{H}_I(t - s) \big] \hat{H}_I(t) \Big\}. \qquad (2.17)$$

A seperatability at all times is now assumed:

$$\hat{\rho}_T(t) = \hat{\rho}_S(t) \otimes \hat{\rho}_E(t), \qquad (2.18)$$

This assumtion has to be made even stronger later $\hat{\rho}_T(t) = \hat{\rho}_S(t) \otimes \hat{\rho}_E(0)$. Expanding Eq. (2.17), we obtain:

$$\dot{\rho}_T(t) = \alpha^2 \int_0^t ds \Big\{ \text{Tr}_E \big[\hat{H}_I(t)\hat{H}_I(t - s)\hat{\rho}_T(t) \big] - \text{Tr}_E \big[\hat{H}_I(t)\hat{\rho}_T(t)\hat{H}_I(t - s) \big] -$$

$$\text{Tr}_E \big[\hat{H}_I(t - s)\hat{\rho}_T(t)\hat{H}_I(t) \big] + \text{Tr}_E \big[\hat{\rho}_T(t)\hat{H}_I(t - s)\hat{H}_I(t) \big] \Big\}. \qquad (2.19)$$

Now, inserting the interaction Hamiltonian by tracking the operators at time $t - s$ with i' and at t with i, we have:

$$\dot{\rho}_T(t) = \alpha^2 \sum_{i,i'} \int_0^t ds \Big\{ \text{Tr}_E \big[\hat{S}_i(t)\hat{S}_{i'}(t - s)\hat{\rho}_S(t) \otimes \hat{E}_i(t)\hat{E}_{i'}(t - s)\hat{\rho}_E(t) \big] -$$

$$\text{Tr}_E \big[\hat{S}_i(t)\hat{\rho}_S(t)\hat{S}_{i'}(t - s) \otimes \hat{E}_i(t)\hat{\rho}_E(t)\hat{E}_{i'}(t - s) \big] -$$

$$\text{Tr}_E \big[\hat{S}_{i'}(t - s)\hat{\rho}_S(t)\hat{S}_i(t) \otimes \hat{E}_{i'}(t - s)\hat{\rho}_E(t)\hat{E}_i(t) \big] +$$

$$\text{Tr}_E \big[\hat{\rho}_S(t)\hat{S}_{i'}(t - s)\hat{S}_i(t) \otimes \hat{\rho}_E(t)\hat{E}_{i'}(t - s)\hat{E}_i(t) \big] \Big\}. \qquad (2.20)$$

Since the trace only acts on the environment, the system operators can be taken out of the trace, and we define the correlation functions:

$$C_{ij}(t - s) = \text{Tr}_E \big[\hat{E}_i(t)\hat{E}_{i'}(t - s)\hat{\rho}_E(t) \big], \qquad (2.21)$$

such that:

$$\dot{\rho}_T(t) = \alpha^2 \sum_{i,i'} \int_0^t ds \Big\{ C_{ij}(t - s) \big[\hat{S}_i(t), \hat{S}_{i'}(t - s)\hat{\rho}_S(t) \big] + \text{H.c.} \Big\}. \qquad (2.22)$$

which is the desired form of the Redfield equation.

Note however, that the we have not used the strong condition $\hat{\rho}_T(t) = \hat{\rho}_S(t) \otimes \hat{\rho}_E(0)$ was not used yet. This however will make it possible to calculate the correlations Eq. (2.21), because we can assume that the enviroment is in a thermal equilibruium at a certain temperature. Because of the assumption this is the case for all times. It is equivalent to say that the environment is unaffected by the system. It is memoryless, because it is very big.

Chapter 3

Bath Correlation Functions

3.1 Bath Correlator

The general task of this chapter is to calculate the bath correlator, which is defined as:

$$C(\tau) = \langle B(\tau)B(0)\rangle, \tag{3.1}$$

where B is the bath operator, specified later. This correlator measures the operator B at two different times in the bath.

3.2 Useful Tools

3.2.1 Infinite Geometric Series

An infinite geometric series is expressed as:

$$S = a + ar + ar^2 + ar^3 + \cdots = \sum_{n=0}^{\infty} ar^n, \tag{3.2}$$

where a is the first term and r is the common ratio. For $|r| < 1$, the sum converges to:

$$S = \frac{a}{1-r}. \tag{3.3}$$

Differentiating Eq. (3.3) with respect to r yields another useful series:

$$\sum_{n=0}^{\infty} nr^n = \frac{r}{(1-r)^2}, \quad \text{for } |r| < 1. \tag{3.4}$$

3.2.2 Trace

For a bipartite system $A \otimes B$, the reduced density matrix of system A is obtained by tracing out system B:

$$\rho_A = \text{Tr}_B[\rho_{AB}], \tag{3.5}$$

where the partial trace over the subspace B is defined as:

$$\text{Tr}_B \left[\sum_{i,j,k,l} |a_i\rangle\langle a_j| \otimes |b_k\rangle\langle b_l| \right] = \sum_{i,j} |a_i\rangle\langle a_j|\text{Tr}\left[|b_k\rangle\langle b_l|\right] \tag{3.6}$$

The expectation value of an operator A in a system S is calculated as:

$$\langle A\rangle_S = \mathrm{Tr}_S[\rho_S A] = \frac{1}{Z}\sum_n e^{-\beta E_n} A_{nn}, \tag{3.7}$$

where the inverse temperature β is defined as:

$$\beta = \frac{1}{k_B T}. \tag{3.8}$$

3.3   Harmonic Oscillators

A bosonic bath is modeled by an infinitely big set of harmonic oscillators, which we assume to be in thermal equilibrium. For such a system the thermal state is described by the Gibbs distribution:

$$\rho = \frac{e^{-\beta H}}{\mathrm{Tr}\left[e^{-\beta H}\right]}, \quad H = \sum_k \hbar\omega_k \left(b_k^\dagger b_k + \frac{1}{2}\right), \quad E_k = \hbar\omega_k(n_k + \frac{1}{2}), \tag{3.9}$$

where ω_k is the frequency of the k-th mode, $b_k^\dagger$ and b_k are the creation and annihilation operators, respectively, and $n_k = \langle b_k^\dagger b_k\rangle$ is the expectation value of the number operator. The number operator is an eigenoperator to the number states $|k\rangle$ and the number n_k represents the number of excitations in that mode. The energy of the k-th mode E_k is directly related to this number.

3.3.1   Single Mode

For a single mode k harmonic oscillator $H = \hbar\omega_k b_k^\dagger b_k$ in thermal equilibrium at temperature T, the density matrix is given by:

$$\rho = \frac{e^{-\beta\hbar\omega_k b_k^\dagger b_k}}{Z_k}, \tag{3.10}$$

where ω_k is the constant frequency of the mode k. The partition function Z can be calculated by the geometric series:

$$Z_k \equiv \mathrm{Tr}\left[e^{-\beta H}\right] = \sum_{m=0}^{\infty}\langle m|e^{-\beta\hbar\omega_k(n_k+\frac{1}{2})}|m\rangle = e^{-\beta\hbar\omega_k/2}\sum_{m=0}^{\infty}\langle m|m\rangle\delta_{km}e^{-\beta\hbar\omega_k n_k} = \frac{e^{-\beta\hbar\omega_k/2}}{1-e^{-\beta\hbar\omega_k}}. \tag{3.11}$$

Using this, the expectation value of the number operator can be calculated:

$$n_k = \langle b_k^\dagger b_k \rangle_{\text{th}} = \text{Tr}\left[b_k^\dagger b_k \frac{e^{-\beta H}}{Z_k} \right] \tag{3.12}$$

$$= \frac{\text{Tr}\left[b_k^\dagger b_k e^{-\beta \hbar \omega_k b_k^\dagger b_k} \right]}{Z_k} \tag{3.13}$$

$$= \frac{\sum_{m=0}^{\infty} \langle m | b_k^\dagger b_k e^{-\beta \hbar \omega_k b_k^\dagger b_k} | m \rangle}{\frac{e^{-\beta \hbar \omega_k/2}}{1 - e^{-\beta \hbar \omega_k}}} \tag{3.14}$$

$$= \frac{e^{-\beta \hbar \omega_k}}{1 - e^{-\beta \hbar \omega_k}} \tag{3.15}$$

$$= \frac{1}{e^{\beta \hbar \omega_k} - 1}. \tag{3.16}$$

where we have used Eq. (3.4) in the last step. The partition function for the infinite set then generalizes to a product:

$$Z = \prod_k Z_k = \prod_k \frac{e^{-\beta \hbar \omega_k/2}}{1 - e^{-\beta \hbar \omega_k}}. \tag{3.17}$$

3.4 Bath Correlators

Now we turn to calculating the bath correlator. The bath operator B is defined as:

$$B = \sum_{n=1}^{\infty} c_n x_n, \tag{3.18}$$

where c_n are coupling constants and x_n are position operators. Note that in Sec. 2.1, the interaction Hamiltonian reduces such that only one bath correlator $C(\tau) \equiv C_{ii}(\tau)$ in Eq. (2.21) remains.

Expressing B in terms of creation and annihilation operators:

$$B(0) = \sum_{n=1}^{\infty} c_n \sqrt{\frac{1}{2 m_n \omega_n}} (b_n + b_n^\dagger), \tag{3.19}$$

$$B(\tau) = \sum_{n=1}^{\infty} c_n \sqrt{\frac{1}{2 m_n \omega_n}} \left(b_n e^{-i \omega_n \tau} + b_n^\dagger e^{i \omega_n \tau} \right). \tag{3.20}$$

Substituting $B(\tau)$ and $B(0)$ into Eq. (3.1), we find:

$$C(\tau) = \left\langle \sum_{n=1}^{\infty} c_n \sqrt{\frac{1}{2 m_n \omega_n}} (b_n e^{-i \omega_n \tau} + b_n^\dagger e^{i \omega_n \tau}) \sum_{m=1}^{\infty} c_m \sqrt{\frac{1}{2 m_m \omega_m}} (b_m + b_m^\dagger) \right\rangle. \tag{3.21}$$

Similar calculations to Eq. (3.12) thermal expectation values can be calculated:

$$\langle b_n b_m^\dagger \rangle = \delta_{nm}(n_n + 1), \quad \langle b_n^\dagger b_m \rangle = \delta_{nm} n_n, \tag{3.22}$$

where n_k is the Bose-Einstein distribution:

$$n_k = \frac{1}{e^{\beta \omega_k} - 1}, \tag{3.23}$$

we obtain:

$$C(\tau) = \sum_{n=1}^{\infty} \frac{c_n^2}{2m_n \omega_n} \left[(n_n + 1)e^{-i\omega_n \tau} + n_n e^{i\omega_n \tau} \right]. \tag{3.24}$$

3.4.1   Spectral Density Representation

The bath correlator can be expressed in terms of the spectral density $J(\omega)$, defined as:

$$J(\omega) = \pi \sum_{n=1}^{\infty} \frac{c_n^2}{2m_n \omega_n} \delta(\omega - \omega_n). \tag{3.25}$$

With this, the bath correlator becomes:

$$C(\tau) = \int_0^{\infty} d\omega \frac{J(\omega)}{\pi} \left[(n(\omega) + 1)e^{-i\omega \tau} + n(\omega)e^{i\omega \tau} \right]. \tag{3.26}$$

3.4.2   Continuum Limit

As the frequencies $\{\omega_j\}$ become dense, the sum transitions to an integral:

$$\sum_{j=1}^{\infty} \quad \longrightarrow \quad \int d\omega' \, \rho(\omega'),$$

where $\rho(\omega')$ is the density of states. The coupling g_j becomes a function of frequency, $g(\omega')$, leading to:

$$J(\omega) = \rho(\omega) \, g(\omega)^2.$$

In this continuum limit, the bath correlator Eq. (3.24) becomes:

$$C(\tau) = \int_0^{\infty} d\omega \frac{J(\omega)}{\pi} \left[\coth\left(\frac{\beta \omega}{2} \right) \cos(\omega \tau) - i \sin(\omega \tau) \right]. \tag{3.27}$$

3.4.3   Ohmic Spectral Density

Source: Ulrich Weiss chapter 7.3: (*my interpretation: The Redfield equation is influenced by classical phenomenological models of dissipation*) For an Ohmic spectral density, the damping is frequency-independent, and the spectral density is given by:

$$J(\omega) \propto \gamma \omega, \tag{3.28}$$

where γ is the damping constant. To ensure physical behavior, a cutoff is introduced:

$$J(\omega) = \eta \frac{\omega^s}{\omega_c^{s-1}} e^{-\omega/\omega_c}, \tag{3.29}$$

where η is a dimensionless coupling constant, ω_c is the cutoff frequency, and s determines the type of spectral density (Ohmic for $s = 1$, sub-Ohmic for $s < 1$, and super-Ohmic for $s > 1$).

Chapter 4

Rabi Oscillations and Related Concepts

4.0.1 Density Matrix Formalism

The density matrix formalism provides a powerful framework to describe the dynamics of quantum systems, especially when dealing with mixed states or decoherence. The density matrix ρ is defined as:

$$\rho = |\psi\rangle\langle\psi|, \tag{4.1}$$

for pure states, and as a statistical mixture for mixed states. In this formalism, the diagonal elements represent populations and the off-diagonal elements represent coherences between states. Coherences are phase relations between different quantum states, which are crucial for interference. For example for a two level system a clear phase relation and a pure quantum state would have off diagonal elements of $\rho_{ij} = 1/2$. This state is often referred to as a coherent superposition of the two states.

When coupling a system to an environment, the environment is responsible for decoherence. The state evolves over time to a purely statistical mixture of states.

The time evolution of the density matrix is governed by the Liouville-von Neumann equation:

$$\frac{\partial \rho}{\partial t} = -\frac{i}{\hbar}[H, \rho], \tag{4.2}$$

where H is the system Hamiltonian.

In the presence of decoherence or dissipation, the dynamics can be described using the Lindblad master equation:

$$\frac{\partial \rho}{\partial t} = -\frac{i}{\hbar}[H, \rho] + \sum_k \mathcal{L}_k(\rho), \tag{4.3}$$

where $\mathcal{L}_k(\rho)$ are Lindblad operators modeling the interaction with the environment.

4.1 Rabi Oscillations

Rabi oscillations describe the coherent oscillatory behavior of a two-level quantum system interacting with a resonant electromagnetic field. This phenomenon is fundamental in quantum mechanics and quantum optics, with applications in quantum computing, spectroscopy, and atomic physics.

4.1.1   1. Schrödinger Picture

Consider a two-level system with states $|g\rangle$ (ground state) and $|e\rangle$ (excited state). The energy separation between the two states is given by:

$$\omega_0 = \frac{E_e - E_g}{\hbar}, \tag{4.4}$$

where E_e and E_g are the energies of the excited and ground states, respectively.

The system Hamiltonian is expressed as:

$$H_S = \hbar\omega_0 |e\rangle \langle e| . \tag{4.5}$$

The interaction of the system with a classical electromagnetic field $E(t)$ is described by the time-dependent interaction Hamiltonian:

$$H_{\text{int}}(t) = -\mu E(t) = - \left(\mu_{eg} |e\rangle \langle g| + \mu_{ge} |g\rangle \langle e| \right) E(t), \tag{4.6}$$

where μ_{eg} and μ_{ge} are the dipole matrix elements.

The total Hamiltonian of the system is then given by:

$$H(t) = H_S + H_{\text{int}}(t), \tag{4.7}$$

which combines the system's intrinsic energy and its interaction with the field.

Alternatively, the total Hamiltonian can be written in terms of Pauli matrices as:

$$H(t) = \frac{\hbar\omega_0}{2}\sigma_z + \hbar\Omega \cos(\omega_L t + \phi)\sigma_x, \tag{4.8}$$

where Ω is the Rabi frequency, proportional to the field amplitude and the dipole matrix element, ϕ, ω_L is the phase, frequency of the driving field respectively, and σ_z and σ_x are the Pauli matrices

The time evolution of the system is governed by the time dependent Schrödinger equation:

$$i\hbar\frac{\partial}{\partial t}|\psi(t)\rangle = H(t)|\psi(t)\rangle, \tag{4.9}$$

which describes the dynamics of the quantum state $|\psi(t)\rangle$ under the influence of the Hamiltonian $H(t)$.

4.1.2   Rotating Wave Approximation (RWA)

The rotating wave approximation simplifies the analysis of the Hamiltonian in Eq. (4.8). This approximation is valid when $\Omega \ll \omega_0$, allowing us to focus on the resonant interaction. The RWA reveals the essence of Rabi oscillations, where the population of the two levels oscillates with the Rabi frequency $\Omega_R = \sqrt{\Delta^2 + \Omega^2}$.

4.2   Applying the RWA Explicitly

Suppose the electric field is classical and oscillatory:

$$E(t) = E_0 \cos(\omega_L t + \phi) = \frac{E_0}{2} \left(e^{i\omega_L t + i\phi} + e^{-i\omega_L t - i\phi} \right) \tag{4.10}$$

Assuming $\mathbf{d} = \mu_{eg} \left| e \right\rangle \left\langle g \right| + \mathbf{d}_{ge} \left| g \right\rangle \left\langle e \right|$ and defining the Rabi frequency:

$$\hbar\Omega = -\mu_{eg} \cdot \mathbf{E}_0 \tag{4.11}$$

is the Rabi frequency, proportional to the field amplitude and the dipole matrix element.
Then the interaction Hamiltonian (4.6) becomes:

$$H_{\text{int}}(t) = \hbar\Omega \cos(\omega_L t + \phi)(\left| e \right\rangle \left\langle g \right| + \left| g \right\rangle \left\langle e \right|) \tag{4.12}$$

Now go to the interaction picture with a unitary transformation $U_0(t)$:

$$U_0(t) = e^{-iH_0 t/\hbar} = e^{-i\omega_0 t \left| e \right\rangle \left\langle e \right|} \tag{4.13}$$

The interaction Hamiltonian in the interaction picture is with Eq. (4.13):

$$H_{\text{int}}^{(I)}(t) = U_0^\dagger(t) H_{\text{int}}(t) U_0(t). \tag{4.14}$$

Under this transformation, the operators evolve as described in Eq. (4.12):

$$\left| e \right\rangle \left\langle g \right| \to e^{i\omega_0 t} \left| e \right\rangle \left\langle g \right|, \quad \left| g \right\rangle \left\langle e \right| \to e^{-i\omega_0 t} \left| g \right\rangle \left\langle e \right|. \tag{4.15}$$

which results in

$$H_{\text{int}}^{(I)}(t) = \hbar\Omega \cos(\omega_L t + \phi) \left(e^{i\omega_0 t} \left| e \right\rangle \left\langle g \right| + e^{-i\omega_0 t} \left| g \right\rangle \left\langle e \right| \right). \tag{4.16}$$

Rotating Frame Transformation

We now define the unitary transformation:

$$U_L(t) = e^{i\omega_L t \left| e \right\rangle \left\langle e \right|} = \begin{pmatrix} 1 & 0 \\ 0 & e^{i\omega_L t} \end{pmatrix} \tag{4.17}$$

that rotates the reference frame of the system to the rotating frame at frequency ω_L.
The transformed density matrix is:

$$\tilde{\rho}(t) = U_L^\dagger(t) \rho(t) U_L(t) \tag{4.18}$$

and in this frame, the total transformed Hamiltonian is:

$$\tilde{H}^I(t) = U_L^\dagger(t) H_{\text{int}}^I(t) U_L(t) - i\hbar U_L(t) \frac{d}{dt} U_L^\dagger(t) \tag{4.19}$$

The second term gives:

$$-i\hbar U_L^\dagger(t) \frac{d}{dt} U_L(t) = -\hbar\omega_L \left| e \right\rangle \left\langle e \right| \tag{4.20}$$

Thus:

$$\tilde{H}^I(t) = -\hbar\omega_L \left| e \right\rangle \left\langle e \right| + U_L^\dagger(t) H_{\text{int}}^I(t) U_L(t) \tag{4.21}$$

Transforming the Interaction Hamiltonian

In the rotating frame:

$$U_L^\dagger(t) \left| e \right\rangle \left\langle g \right| U_L(t) = e^{-i\omega_L t} \left| e \right\rangle \left\langle g \right|, \quad U_L^\dagger(t) \left| g \right\rangle \left\langle e \right| U_L(t) = e^{i\omega_L t} \left| g \right\rangle \left\langle e \right| \tag{4.22}$$

The interaction Hamiltonian becomes:

$$\tilde{H}_{\text{int}}(t) = -\hbar\Omega\cos(\omega_L t + \phi)\left(e^{i(\omega_0 - \omega_L)t}\left|e\right\rangle\left\langle g\right| + e^{-i(\omega_0 - \omega_L)t}\left|g\right\rangle\left\langle e\right|\right) \tag{4.23}$$

Rotating Wave Approximation (RWA)

We can use the identity:

$$\cos(\omega_L t + \phi) = \frac{1}{2}\left(e^{i(\omega_L t + \phi)} + e^{-i(\omega_L t + \phi)}\right) \tag{4.24}$$

Under RWA, drop fast-rotating terms $e^{\pm i2\omega_L t}$, keeping only:

$$\tilde{H}_{\text{RWA}} = -\hbar\Delta\left|e\right\rangle\left\langle e\right| - \frac{E_0}{2}\left(\mu_{eg}\left|e\right\rangle\left\langle g\right| + \mu_{ge}\left|g\right\rangle\left\langle e\right|\right) \tag{4.25}$$

Equation of Motion

The von Neumann equation becomes:

$$\frac{d}{dt}\tilde{\rho}(t) = -\frac{i}{\hbar}[\tilde{H}_{\text{RWA}}, \tilde{\rho}(t)] + (\text{dissipation terms}) \tag{4.26}$$

To recover the entries of the original density matrix $\rho(t)$ from the evolved density matrix in the rotating frame $\tilde{\rho}(t)$, we use the inverse of the unitary transformation $U_L(t)$:

$$\rho(t) = U_L^\dagger(t)\tilde{\rho}(t)U_L(t) \tag{4.27}$$

where $U_L(t)$ and $U_L^\dagger(t)$ are given in Eq. (4.17).

Let the density matrices be:

$$\rho(t) = \begin{pmatrix} \rho_{gg}(t) & \rho_{ge}(t) \\ \rho_{eg}(t) & \rho_{ee}(t) \end{pmatrix}, \quad \tilde{\rho}(t) = \begin{pmatrix} \tilde{\rho}_{gg}(t) & \tilde{\rho}_{ge}(t) \\ \tilde{\rho}_{eg}(t) & \tilde{\rho}_{ee}(t) \end{pmatrix} \tag{4.28}$$

The recovery process is:

$$\rho(t) = \begin{pmatrix} 1 & 0 \\ 0 & e^{-i\omega_L t} \end{pmatrix}\begin{pmatrix} \tilde{\rho}_{gg}(t) & \tilde{\rho}_{ge}(t) \\ \tilde{\rho}_{eg}(t) & \tilde{\rho}_{ee}(t) \end{pmatrix}\begin{pmatrix} 1 & 0 \\ 0 & e^{i\omega_L t} \end{pmatrix} \tag{4.29}$$

Simplifying:

$$\rho(t) = \begin{pmatrix} \tilde{\rho}_{gg}(t) & e^{i\omega_L t}\tilde{\rho}_{ge}(t) \\ e^{-i\omega_L t}\tilde{\rho}_{eg}(t) & \tilde{\rho}_{ee}(t) \end{pmatrix} \tag{4.30}$$

Thus, the entries of the original density matrix $\rho(t)$ are related to the entries of the density matrix in the rotating frame $\tilde{\rho}(t)$ by:

$$\rho_{gg}(t) = \tilde{\rho}_{gg}(t)$$
$$\rho_{ee}(t) = \tilde{\rho}_{ee}(t)$$
$$\rho_{ge}(t) = e^{i\omega_L t}\tilde{\rho}_{ge}(t)$$
$$\rho_{eg}(t) = e^{-i\omega_L t}\tilde{\rho}_{eg}(t)$$

By moving to a rotating frame and neglecting rapidly oscillating terms, the effective Hamiltonian becomes:

$$H_{\text{RWA}} = \frac{\hbar\Delta}{2}\sigma_z + \frac{\hbar\Omega}{2}\sigma_x, \tag{4.31}$$

4.3 Applications and Implications

Rabi oscillations and the associated theoretical tools, such as the RWA and density matrix formalism, have wide-ranging applications:

- **Quantum Computing:** Rabi oscillations are used to implement quantum gates by precisely controlling the population of qubits.

- **Spectroscopy:** The Rabi frequency provides information about the interaction strength between light and matter.

- **Atomic Physics:** Understanding Rabi oscillations is essential for manipulating atomic states in experiments.

These concepts form the foundation for advanced topics in quantum mechanics and quantum technologies.

Step-by-Step Derivation of RWA in a Two-Level System (with Phase)

Step 5: Apply the Rotating Wave Approximation (RWA)

Use the identity:

$$\cos(\omega_L t + \phi) = \frac{1}{2}\left(e^{i(\omega_L t + \phi)} + e^{-i(\omega_L t + \phi)}\right) \tag{4.32}$$

The interaction terms become:

$$\frac{\hbar\Omega}{2}\left(e^{i(\omega_0 t + \omega_L t + \phi)}\,|e\rangle\langle g| + e^{i(\omega_0 t - \omega_L t - \phi)}\,|e\rangle\langle g| + \text{h.c.}\right) \tag{4.33}$$

Keep only the **slowly rotating terms** at frequency $\Delta = \omega_0 - \omega_L$, and drop the fast ones. The RWA Hamiltonian becomes:

$$H_{\text{RWA}} = \hbar\Delta\,|e\rangle\langle e| + \frac{\hbar\Omega}{2}\left(e^{i\phi}\,|e\rangle\langle g| + e^{-i\phi}\,|g\rangle\langle e|\right) \tag{4.34}$$

Step 6: Solve the Dynamics (Rabi Oscillations with Phase)

In matrix form, in the basis $\{|e\rangle, |g\rangle\}$:

$$H_{\text{RWA}} = \frac{\hbar}{2}\begin{pmatrix} 2\Delta & \Omega e^{i\phi} \\ \Omega e^{-i\phi} & 0 \end{pmatrix} \tag{4.35}$$

The phase ϕ does not change the **Rabi frequency**:

$$\Omega_R = \sqrt{\Delta^2 + \Omega^2} \tag{4.36}$$

But it **rotates the axis of Rabi oscillations** in the Bloch sphere — i.e., it changes the **initial direction** of the drive.

Chapter 5

Numerical Implementation of Two-Dimensional Electronic Spectroscopy

This chapter presents the computational framework developed for simulating two-dimensional electronic spectroscopy (2DES) spectra of molecular systems. The implementation focuses on the technical aspects of quantum system evolution, pulse sequence generation, data processing, and visualization, providing a bridge between the theoretical framework established in previous chapters and practical computational methods.

5.1 Overview of Simulation Architecture

The simulation framework follows a modular structure that separates quantum mechanical evolution from spectroscopic data processing. The general workflow consists of:

1. Definition of quantum system parameters (energy levels, dipole moments, coupling strengths)

2. Generation of pulse sequences with specific time delays and phases

3. Evolution of the density matrix under pulse influences and environmental coupling

4. Calculation of the system's polarization response

5. Processing of time-domain data to obtain frequency-domain 2D spectra

6. Averaging over inhomogeneous distributions and phase cycling

This modular approach enables systematic investigation of different physical parameters while maintaining computational efficiency through parallel processing capabilities.

5.2 Computing Two-Dimensional Polarization Response

The core calculation computes the third-order polarization response by iterating through coherence times (τ_{coh}) and detection times (t_{det}) for a given waiting time (T_{wait}):

$$P^{(3)}(\tau_{\text{coh}}, T_{\text{wait}}, t_{\text{det}}) = \text{Tr}[\hat{\mu} \cdot \hat{\rho}^{(3)}(\tau_{\text{coh}}, T_{\text{wait}}, t_{\text{det}})] \tag{5.1}$$

where $\hat{\mu}$ is the dipole operator and $\hat{\rho}^{(3)}$ is the third-order density matrix. This calculation implements the three-pulse sequence through sequential evolution steps:

1. Apply the first pulse with phase ϕ_0 and evolve for coherence time τ_{coh}

2. Apply the second pulse with phase ϕ_1 and evolve for waiting time T_{wait}

3. Apply the third pulse with phase ϕ_2 and measure response during detection time t_{det}

The temporal evolution utilizes either custom equations derived from literature or standard quantum dynamics solvers from the QuTiP library, ensuring both flexibility and computational accuracy.

5.3   Inhomogeneous Broadening Implementation

To accurately model molecular systems, the simulation accounts for inhomogeneous broadening by averaging over a distribution of transition frequencies. The distribution follows a Gaussian profile:

$$\sigma(E - E_0) = \frac{1}{\sigma_{\text{val}}\sqrt{2\pi}} \exp\left(-\frac{(E - E_0)^2}{2\sigma_{\text{val}}^2}\right) \tag{5.2}$$

where $\sigma_{\text{val}} = \Delta/(2\sqrt{2\ln 2})$ relates the standard deviation to the full width at half maximum Δ.

The sampling from this distribution employs a rejection sampling algorithm that ensures accurate representation of the broadening profile while maintaining computational efficiency. The algorithm operates by:

1. Defining the sampling range $[E_{\text{min}}, E_{\text{max}}] = [E_0 - E_{\text{range}} \cdot \Delta, E_0 + E_{\text{range}} \cdot \Delta]$

2. Computing the maximum value σ_{max} of $\sigma(E)$ in the range

3. Generating candidate values uniformly and accepting them based on the probability density

4. Repeating until the desired number of samples is obtained

5.4   Parallel Processing of Parameter Combinations

The computationally intensive nature of 2DES simulations, particularly when averaging over frequency samples and phase combinations, necessitates efficient parallel processing. The averaged response is calculated as:

$$\langle P^{(3)}(\tau_{\text{coh}}, T_{\text{wait}}, t_{\text{det}})\rangle = \frac{1}{N_\omega N_\phi} \sum_{i=1}^{N_\omega} \sum_{j=1}^{N_\phi} P^{(3)}_{\omega_i, \phi_j}(\tau_{\text{coh}}, T_{\text{wait}}, t_{\text{det}}) \tag{5.3}$$

where N_ω represents the number of frequency samples and N_ϕ the number of phase combinations. The implementation utilizes Python's `ProcessPoolExecutor` to distribute calculations across available CPU cores, significantly reducing computation time for parameter sweeps.

5.5   Fourier Transformation and Spectral Analysis

The conversion from time-domain to frequency-domain spectra utilizes two-dimensional Fourier transformation:

$$S(\omega_\tau, \omega_t) = \int_{-\infty}^{\infty} \int_{-\infty}^{\infty} P^{(3)}(\tau, T, t)e^{-i\omega_\tau \tau}e^{-i\omega_t t}\, d\tau\, dt \tag{5.4}$$

In the discrete implementation, this becomes a Fast Fourier Transform (FFT) operation:

$$S[k,l] = \sum_{m=0}^{M-1} \sum_{n=0}^{N-1} P^{(3)}[m,n] \exp\left(-i\frac{2\pi km}{M}\right) \exp\left(-i\frac{2\pi ln}{N}\right) \tag{5.5}$$

The frequency axes are converted to wavenumber units (10^4 cm^{-1}) using:

$$\nu = \frac{f}{c} \times 10^4 \text{ cm}^{-1} \tag{5.6}$$

where f is the frequency in cycles/fs and $c = 2.998 \times 10^{-5}$ cm/fs is the speed of light.

5.6 Data Processing and Visualization

The 2D spectra visualization system represents different aspects of the complex-valued data:

- Real part: Absorptive component containing peak positions

- Imaginary part: Dispersive component providing line shape information

- Absolute value: Overall signal strength

- Phase: Phase relationship between excitation and detection processes

For data containing both positive and negative values, a custom white-centered colormap enhances visualization of signal features. The normalization scheme:

$$\text{data}_{\text{normalized}} = \frac{\text{data}}{\max(|\text{data}|)} \tag{5.7}$$

ensures consistent visualization across different parameter sets while preserving relative signal amplitudes.

5.7 Extending Time and Frequency Axes

To improve Fourier transform resolution and reduce artifacts from finite sampling, the implementation supports zero-padding of time-domain data:

$$\text{data}_{\text{extended}} = \begin{bmatrix} 0 & \cdots & 0 & \text{data} & 0 & \cdots & 0 \end{bmatrix} \tag{5.8}$$

The corresponding time axes extend proportionally:

$$t_{\text{extended}} = \{t_0 - n_{\text{pre}}\Delta t, \ldots, t_0, \ldots, t_N, \ldots, t_N + n_{\text{post}}\Delta t\} \tag{5.9}$$

where n_{pre} and n_{post} represent the number of zero-padded points before and after the original data.

5.8 Global Data Combination for Multiple Waiting Times

For studies of temporal evolution in coherence phenomena, the simulation supports scanning over multiple waiting times. The local time and frequency data are mapped to global axes through:

$$\text{global\_data}[\text{idx}_\tau, \text{idx}_t] + = \text{local\_data}[\text{local\_idx}_\tau, \text{local\_idx}_t] \tag{5.10}$$

where idx_τ and idx_t represent indices in the global arrays corresponding to local values of τ_{coh} and t_{det}. The global data normalization:

$$\mathrm{global\_data}_{\mathrm{normalized}} = \frac{\mathrm{global\_data}}{N_{T_{\mathrm{wait}}}} \tag{5.11}$$

produces the average spectrum over all waiting times, enabling analysis of relaxation and dephasing processes.

5.9   Connection to Theoretical Framework

The numerical implementation directly implements the theoretical concepts established in previous chapters:

- Quantum system evolution follows the Redfield master equation for open quantum systems (Chapter **??**)

- Polarization calculations implement the nonperturbative approach for 2DES theory

- Spectral analysis methods extract signatures of quantum coherence in biological systems

- Environmental coupling effects are incorporated through systematic parameter studies

This computational framework provides a robust platform for simulating 2DES spectra of complex molecular systems and extracting quantum dynamical parameters relevant to biological function.

5.10   Validation and Performance Considerations

The implementation includes validation procedures comparing simulation results against analytical solutions for simple systems. Performance optimization through vectorized operations and parallel processing enables parameter sweeps necessary for comprehensive system characterization.

Special considerations for biological systems include:

1. Larger inhomogeneous broadening due to complex environments

2. Faster dephasing from environmental coupling

3. Multiple chromophore contributions to the signal

4. Energy transfer processes on various timescales

The simulation framework accommodates these aspects through customizable system parameters and flexible averaging procedures, providing a versatile tool for investigating quantum coherence phenomena in biological systems.

Chapter 6

Principles of Spectroscopy

6.1 Fundamentals of Spectroscopy

Spectroscopy, in its broadest definition, is the study of the interaction between matter and electromagnetic radiation as a function of wavelength or frequency [9]. This powerful analytical technique provides insights into the composition, structure, and dynamics of physical systems by examining how they absorb, emit, or scatter light. The fundamental principle underlying all spectroscopic methods is that each atom, molecule, or complex system has a unique set of energy levels, and transitions between these levels involve the absorption or emission of photons with specific energies [10].

6.1.1 Basic Principles

The foundation of spectroscopy rests on the quantization of energy in atomic and molecular systems. According to quantum mechanics, atoms and molecules can exist only in discrete energy states [11]. The energy difference between two states, ΔE, determines the frequency ν or wavelength λ of light that can be absorbed or emitted during a transition between these states, following Planck's relation:

$$\Delta E = h\nu = \frac{hc}{\lambda} \tag{6.1}$$

where h is Planck's constant and c is the speed of light. This relation forms the basis for spectroscopic analysis, allowing researchers to probe the energy structure of matter by observing the spectrum of absorbed or emitted radiation.

6.1.2 Classification of Spectroscopic Techniques

Spectroscopic methods can be categorized based on various criteria:

- **Nature of the interaction:** Absorption, emission, scattering, reflection

- **Frequency range:** Radio-frequency, microwave, terahertz, infrared, visible, ultraviolet, X-ray, gamma-ray

- **Type of energy transition:** Electronic, vibrational, rotational, nuclear

- **Number of photons involved:** Linear (one-photon) vs. nonlinear (multi-photon) spectroscopy

Each spectroscopic technique provides different information about the system under study. For instance, rotational spectroscopy reveals molecular geometry, vibrational spectroscopy elucidates bonding patterns, and electronic spectroscopy probes electronic structure and excited state dynamics.

6.1.3   Time Scales in Spectroscopy

Different spectroscopic methods operate on different time scales, allowing the investigation of processes ranging from ultrafast electronic motions to slow conformational changes [12, 13]:

- Femtosecond (10^{-15} s): Electronic transitions, vibrational coherences

- Picosecond (10^{-12} s): Vibrational relaxation, rotational motion

- Nanosecond (10^{-9} s): Fluorescence lifetimes, energy transfer

- Microsecond to millisecond (10^{-6} to 10^{-3} s): Chemical reactions, protein folding

The development of ultrafast laser systems has revolutionized spectroscopy by allowing direct observation of molecular dynamics on femtosecond time scales, leading to the field of femtochemistry and ultrafast spectroscopy.

6.2   Nonlinear Optics

Nonlinear optics deals with phenomena that occur when the response of a material to an applied optical field depends nonlinearly on the strength of the field [10]. This nonlinearity becomes significant at high light intensities, such as those provided by pulsed lasers.

6.2.1   Linear vs. Nonlinear Optical Response

In the linear regime, the induced polarization $\vec{P}$ in a material is directly proportional to the applied electric field $\vec{E}$:

$$\vec{P} = \varepsilon_0 \chi^{(1)} \vec{E} \tag{6.2}$$

where ε_0 is the vacuum permittivity and $\chi^{(1)}$ is the linear susceptibility tensor. This relationship describes phenomena such as refraction and absorption.
In the nonlinear regime, the polarization can be expressed as a power series in the electric field:

$$\vec{P} = \varepsilon_0 (\chi^{(1)} \vec{E} + \chi^{(2)} \vec{E}^2 + \chi^{(3)} \vec{E}^3 + \ldots) \tag{6.3}$$

where $\chi^{(2)}$ and $\chi^{(3)}$ are the second- and third-order nonlinear susceptibility tensors, respectively. These higher-order terms give rise to a variety of nonlinear optical phenomena.

6.2.2   Second-Order Nonlinear Processes

Second-order nonlinear processes, governed by the $\chi^{(2)}$ term, occur only in non-centrosymmetric materials (those lacking inversion symmetry). Important second-order effects include:

- **Second Harmonic Generation (SHG):** Two photons of frequency ω combine to generate a photon of frequency 2ω.

- **Sum Frequency Generation (SFG):** Two photons of frequencies ω_1 and ω_2 combine to produce a photon of frequency $\omega_1 + \omega_2$.

- **Difference Frequency Generation (DFG):** Two photons of frequencies ω_1 and ω_2 interact to create a photon of frequency $\omega_1 - \omega_2$.

- **Optical Parametric Amplification (OPA):** A pump photon of frequency ω_p splits into signal (ω_s) and idler (ω_i) photons, such that $\omega_p = \omega_s + \omega_i$.

6.2.3   Third-Order Nonlinear Processes

Third-order nonlinear processes, governed by the $\chi^{(3)}$ term, can occur in all materials, regardless of symmetry. Key third-order effects include:

- **Third Harmonic Generation (THG):** Three photons combine to generate a photon of tripled frequency.

- **Four-Wave Mixing (FWM):** Four photons interact, satisfying energy conservation.

- **Nonlinear Refraction:** The refractive index depends on light intensity (Kerr effect).

- **Two-Photon Absorption (TPA):** Simultaneous absorption of two photons to excite a transition.

These third-order processes form the basis for many nonlinear spectroscopic techniques, including pump-probe spectroscopy, transient grating, and various multidimensional spectroscopies.

6.2.4   Four-Level System Model for Third-Order Spectroscopy

The four-level system represents the minimal complete model for describing third-order nonlinear spectroscopic phenomena [14, 15]. While simpler models such as two-level systems (TLS) are sufficient for understanding linear spectroscopy and some basic nonlinear effects, they cannot fully capture all pathways contributing to third-order signals like those in 2D electronic spectroscopy or photon echo experiments.

In a typical four-level system, the energy states include:

- $|g\rangle$: Ground state

- $|e_1\rangle$ and $|e_2\rangle$: First excited states (single excitons)

- $|f\rangle$: Doubly excited state (two excitons)

This configuration allows modeling of all possible Liouville pathways that contribute to the third-order response function [16]. The inclusion of multiple excited states and a doubly excited state is essential for describing phenomena such as ground-state bleaching, stimulated emission, and excited-state absorption—the three primary components of signals observed in techniques like transient absorption and 2D electronic spectroscopy.

The third-order polarization $P^{(3)}$ in such a system can be expressed as a sum of different pathways:

$$P^{(3)} = P^{(3)}_{GSB} + P^{(3)}_{SE} + P^{(3)}_{ESA} + \ldots \tag{6.4}$$

where GSB, SE, and ESA represent ground-state bleaching, stimulated emission, and excited-state absorption, respectively. The line-broadening function formalism within this four-level model enables detailed analysis of spectral lineshapes and system-bath interactions [14, 15]. While two-level systems are pedagogically valuable and simplify certain calculations, the four-level model captures the richness of nonlinear spectroscopic signals and serves as the foundation for interpreting complex experiments such as multidimensional spectroscopy.

6.2.5 Optical Bloch Equations

The interaction of light with matter in nonlinear spectroscopy is often described using the density matrix formalism and the optical Bloch equations [17]. For a simple two-level system, the density matrix elements ρ_{ij} evolve according to:

$$\frac{d\rho_{11}}{dt} = -i\frac{\mu_{12}E(t)}{\hbar}(\rho_{21} - \rho_{12}) - \Gamma_1\rho_{11} \tag{6.5}$$

$$\frac{d\rho_{12}}{dt} = -i\omega_{12}\rho_{12} - i\frac{\mu_{12}E(t)}{\hbar}(\rho_{22} - \rho_{11}) - \Gamma_2\rho_{12} \tag{6.6}$$

where ω_{12} is the transition frequency, μ_{12} is the transition dipole moment, $E(t)$ is the electric field, and Γ_1 and Γ_2 are the population relaxation and decoherence rates, respectively. These equations can be extended to describe more complex systems and higher-order nonlinear responses.

6.3 Wavevector Phase-Matching Conditions

Phase-matching is a crucial concept in nonlinear optics that determines the efficiency and directionality of nonlinear optical processes [10, 18]. It ensures that the generated signal field constructively interferes throughout the interaction medium.

6.3.1 Physical Meaning of Phase-Matching

In nonlinear optical processes, multiple light waves interact within a material to generate new frequencies. For these processes to be efficient, the phase relationship between the interacting waves must be maintained throughout the propagation distance. This condition is known as phase-matching.

Physically, phase-matching represents momentum conservation in the photon picture. For a general nonlinear process, the wavevector of the generated signal $(\vec{k}_s)$ is determined by the vector sum of the input wavevectors:

$$\vec{k}_s = \pm\vec{k}_1 \pm \vec{k}_2 \pm \vec{k}_3 \pm \ldots \tag{6.7}$$

The signs depend on whether the corresponding field acts as a "bra" $(-)$ or a "ket" $(+)$ in the quantum mechanical description, which corresponds to photon emission or absorption, respectively.

6.3.2 Phase-Matching in Four-Wave Mixing

Four-wave mixing (FWM) is a third-order nonlinear process that plays a central role in many spectroscopic techniques. In a typical FWM experiment, three input fields with wavevectors $\vec{k}_1$, $\vec{k}_2$, and $\vec{k}_3$ generate a signal in the direction $\vec{k}_s$ given by:

$$\vec{k}_s = \pm\vec{k}_1 \pm \vec{k}_2 \pm \vec{k}_3 \tag{6.8}$$

Different combinations of signs correspond to different phase-matching conditions, leading to signals in different spatial directions. These distinct signal directions allow separation of various nonlinear optical processes.

6.3.3 Rephasing and Non-Rephasing Signals

In the context of multidimensional spectroscopy, phase-matched signals are often classified into rephasing and non-rephasing contributions [14, 19]:

- **Rephasing signals** follow the phase-matching condition $\vec{k}_s = -\vec{k}_1 + \vec{k}_2 + \vec{k}_3$. During the evolution period between the first and second interactions, the phase accumulated due to different frequencies can be reversed during the period between the third interaction and signal emission. This leads to a photon echo effect.

- **Non-rephasing signals** satisfy $\vec{k}_s = +\vec{k}_1 - \vec{k}_2 + \vec{k}_3$. In this case, the phase evolution continues in the same direction, and no echo is formed.

The combination of rephasing and non-rephasing signals provides comprehensive information about the system's energy structure and dynamics.

6.3.4 Phase Cycling in Nonlinear Spectroscopy

While phase-matching enables the spatial isolation of desired nonlinear signals, phase cycling provides an alternative or complementary approach by distinguishing signals based on their phase characteristics rather than their spatial propagation directions [20, 21]. This technique is particularly valuable in experiments where spatial isolation is impractical, such as in collinear beam geometries or when studying samples with significant scattering.

In phase cycling, multiple measurements are taken with systematically varied phases of the excitation pulses. The desired nonlinear signals can then be extracted through appropriate linear combinations of these measurements. The fundamental principle relies on the fact that different nonlinear pathways respond distinctly to changes in the phases of the input fields.

For a third-order signal generated by three excitation pulses with phases ϕ_1, ϕ_2, and ϕ_3, the phase of the resulting signal depends on the specific pathway:

$$\phi_s = \pm\phi_1 \pm \phi_2 \pm \phi_3 \tag{6.9}$$

By varying the input phases through a complete cycle (typically in steps of $\pi/2$) and applying discrete Fourier transform methods to the collected data, specific pathways can be isolated based on their unique phase dependencies.

Figure 6.1: Comparison of experimental setups for (a) phase-matching-based signal detection using non-collinear beam geometry and (b) phase cycling-based signal isolation using collinear geometry. Phase cycling allows for simpler experimental setups at the cost of requiring multiple measurements with varied pulse phases.

A common implementation is the 4-step phase cycling procedure, where each input pulse phase is cycled through values of $\{0, \pi/2, \pi, 3\pi/2\}$. For three-pulse experiments, this results in 64 possible phase combinations, although in practice, a reduced set is often sufficient to isolate signals of interest.

Phase cycling offers several advantages:

- It allows for simpler optical setups with collinear or partially collinear beam geometries

- It enables effective background suppression, particularly of scatter and lower-order contributions

- It facilitates the separation of rephasing and non-rephasing pathways within the same measurement series

- It can be implemented in experimental setups where traditional phase-matching is challenging, such as in multidimensional infrared spectroscopy

In modern multidimensional spectroscopy, phase cycling is often combined with phase-matching to achieve optimal signal isolation and background suppression [20, 22].

6.4   Photon Echo Spectroscopy

Photon echo spectroscopy is a powerful nonlinear optical technique used to eliminate inhomogeneous broadening and probe dynamic processes in complex systems [9, 23]. It represents a time-domain analog of spectral hole-burning.

6.4.1   Principle of Photon Echo

The photon echo phenomenon arises from the rephasing of coherences in an ensemble of quantum systems. In the simplest case of a two-pulse photon echo:

1. The first pulse creates a coherent superposition between ground and excited states.

2. During a waiting period τ, the coherences evolve at different frequencies due to inhomogeneous broadening, resulting in phase dispersion.

3. The second pulse, applied at time τ after the first, effectively reverses the phase evolution of the coherences.

4. At time 2τ, the phases realign (rephase), producing a macroscopic polarization that emits an echo signal.

The echo intensity as a function of the delay time τ reveals information about the dephasing processes in the system.

6.4.2   Three-Pulse Photon Echo

The three-pulse photon echo extends the basic two-pulse technique by introducing a population period. The pulse sequence is as follows:

1. The first pulse creates coherences.

2. After time τ, the second pulse converts these coherences to populations.

3. During a waiting time T, population relaxation and spectral diffusion can occur.

4. The third pulse, applied at time T after the second, reconverts populations to coherences.

5. At time τ after the third pulse, the echo signal is emitted.

By scanning the waiting time T, this technique allows measurement of population dynamics and spectral diffusion processes.

6.4.3 Two-Dimensional Electronic Spectroscopy

Two-dimensional electronic spectroscopy (2DES) represents the state-of-the-art in photon echo techniques [19, 24, 25]. It correlates excitation and detection frequencies, revealing couplings between different transitions and energy transfer pathways.

In 2DES, the delay time τ between the first and second pulses is systematically varied, and the signal field is detected in a phase-resolved manner using spectral interferometry [26, 27]. Fourier transformation with respect to τ yields the excitation frequency axis (ω_τ), while spectral resolution of the signal provides the detection frequency axis (ω_t).

The resulting 2D spectrum contains peaks along the diagonal ($\omega_\tau = \omega_t$) corresponding to the linear absorption spectrum, while off-diagonal peaks reveal couplings and energy transfer between different states. The evolution of the 2D spectra with waiting time T provides detailed information about energy transfer kinetics, spectral diffusion, and quantum coherence effects.

$$S(\omega_\tau, T, \omega_t) = \iint dt\, d\tau\, e^{i\omega_t t} e^{-i\omega_\tau \tau} S(t, T, \tau) \tag{6.10}$$

where $S(t, T, \tau)$ is the time-domain signal.

6.4.4 Heterodyne and Homodyne Detection

The detection scheme plays a crucial role in nonlinear spectroscopy, affecting both the sensitivity and the information content of the measurements. Two primary detection methods are employed in multidimensional spectroscopy: homodyne and heterodyne detection [22, 26].

Homodyne Detection

In homodyne detection, the intensity of the emitted signal field is measured directly:

$$S_{\text{homodyne}} \propto |E_{\text{sig}}|^2 \propto |P^{(3)}|^2 \tag{6.11}$$

where E_{sig} is the signal electric field and $P^{(3)}$ is the third-order polarization. While experimentally simpler, homodyne detection has several limitations:

- It measures only the signal intensity, losing phase information

- The signal scales as the square of the third-order response

- Background-free detection requires careful phase-matching

- It is more susceptible to noise at low signal levels

Heterodyne Detection

Heterodyne detection involves the interference of the signal field with a reference field (local oscillator, LO) of known amplitude and phase:

$$S_{\text{heterodyne}} \propto |E_{\text{sig}} + E_{\text{LO}}|^2 \approx |E_{\text{LO}}|^2 + 2|E_{\text{LO}}||E_{\text{sig}}|\cos(\phi_{\text{LO}} - \phi_{\text{sig}}) + |E_{\text{sig}}|^2 \tag{6.12}$$

Since $|E_{\text{LO}}| \gg |E_{\text{sig}}|$, the cross-term dominates, and the signal can be extracted by phase-cycling or lock-in detection. Heterodyne detection offers several advantages [26]:

- It provides both amplitude and phase information of the signal

- The signal scales linearly with the third-order response

- It offers enhanced sensitivity through amplification by the local oscillator

- It allows for a more direct connection to theoretical models

In modern multidimensional spectroscopy, spectral interferometry—a form of heterodyne detection—is widely employed [23]. The signal field and a time-delayed reference pulse are spatially overlapped and spectrally resolved using a spectrometer. The resulting interferogram in the frequency domain contains the complete information about the signal field's amplitude and phase.

6.4.5   Applications of Photon Echo Spectroscopy

Photon echo techniques have been applied to a wide range of problems across chemistry, biology, and materials science:

- **Exciton dynamics** in photosynthetic complexes, revealing quantum coherent energy transfer pathways [25, 28]

- **Vibrational dynamics** in proteins and liquids, elucidating structural fluctuations and hydrogen-bonding networks [29]

- **Charge transfer processes** in organic photovoltaics and light-harvesting systems

- **Coupling mechanisms** between electronic and vibrational degrees of freedom [30]

The ability of these techniques to separate homogeneous and inhomogeneous broadening, while providing time-resolved information about energy transfer and dephasing processes, makes them indispensable tools in modern physical chemistry and biophysics.

6.5   Advanced Spectroscopic Methods

Building upon the principles discussed in previous sections, several advanced spectroscopic techniques have been developed to address specific scientific questions. These methods combine the principles of nonlinear optics, phase-matching, and coherence phenomena to provide unprecedented insights into complex systems.

6.5.1   Multidimensional Infrared Spectroscopy

Similar to 2DES, two-dimensional infrared (2DIR) spectroscopy correlates vibrational transitions, providing information about molecular structure, conformational dynamics, and vibrational coupling [29, 30]. The technique is particularly powerful for studying hydrogen bonding networks, protein secondary structure, and chemical reaction dynamics.
In 2DIR, cross-peaks between different vibrational modes reveal anharmonic coupling and energy transfer pathways, while the lineshapes encode information about structural heterogeneity and dynamics [30]. Time-resolved 2DIR further allows tracking of structural changes during chemical reactions or conformational transitions [13].

6.5.2   Coherent Raman Techniques

Coherent anti-Stokes Raman scattering (CARS) and stimulated Raman scattering (SRS) are nonlinear optical techniques that provide enhanced sensitivity compared to spontaneous Raman spectroscopy [10]. These methods are widely used for chemically-specific microscopy without fluorescent labels.

In CARS, three fields with frequencies ω_1, ω_2, and ω_3 generate a signal at frequency $\omega_s = \omega_1 - \omega_2 + \omega_3$ when the frequency difference $\omega_1 - \omega_2$ matches a vibrational resonance. The coherent nature of the process leads to signal enhancement compared to spontaneous Raman scattering.

6.5.3 Transient Absorption Spectroscopy

Transient absorption spectroscopy, also known as pump-probe spectroscopy, is a powerful technique for studying excited-state dynamics [31]. In this method, a short pump pulse excites the sample, and a subsequent probe pulse measures the resulting changes in absorption as a function of the time delay between the pulses.

The transient absorption signal ΔA can be expressed as:

$$\Delta A(t, \lambda) = -\log\left(\frac{I_{\text{pump-on}}(t, \lambda)}{I_{\text{pump-off}}(\lambda)}\right) \tag{6.13}$$

where $I_{\text{pump-on}}$ and $I_{\text{pump-off}}$ represent the transmitted probe intensity with and without the pump pulse, respectively.

Features in transient absorption spectra include ground-state bleaching, stimulated emission, excited-state absorption, and product absorption. Each of these contributions reflects different physical processes [32, 33]:

- **Ground-State Bleaching (GSB):** The pump pulse depletes the ground state population, resulting in decreased absorption of the probe pulse from the ground state. This appears as a negative signal in transient absorption spectra, coinciding spectrally with the ground-state absorption.

- **Stimulated Emission (SE):** When the probe pulse interacts with molecules in the excited state, it can stimulate emission back to the ground state. This process also yields a negative signal, typically red-shifted relative to the GSB due to the Stokes shift.

- **Excited-State Absorption (ESA):** Molecules in the excited state can absorb the probe pulse, transitioning to even higher excited states. This process yields a positive signal in the transient absorption spectrum, as it represents additional absorption that occurs only when the sample is excited.

Figure 6.2 illustrates these three primary contributions to transient absorption signals.

Analysis of these features as a function of time delay provides information about excited-state lifetimes, energy transfer processes, and photochemical reaction pathways. The ability to separate and identify these contributions is crucial for understanding the dynamics of complex molecular systems [32, 33].

6.6 Summary and Outlook

Spectroscopy continues to evolve as a cornerstone analytical technique in physical sciences [9, 14]. From the basic principles of light-matter interaction to advanced nonlinear methods, spectroscopic approaches provide unique insights into the structure, dynamics, and function of complex systems across multiple time and length scales.

Recent developments in laser technology, detection methods, and theoretical frameworks have expanded the frontiers of spectroscopy [19, 31]. Attosecond spectroscopy now probes electron dynamics on their natural time scale, while quantum light sources open new possibilities for quantum-enhanced measurements.
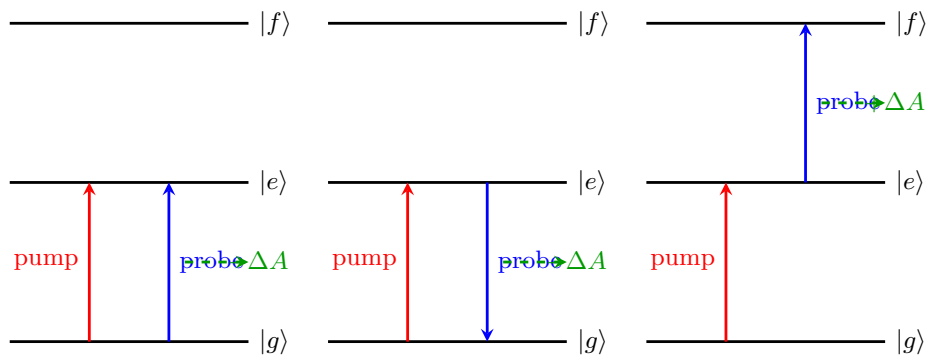
(a) Ground-State Bleaching (b) Stimulated Emission (c) Excited-State Absorption

Figure 6.2: Schematic representation of the three primary contributions to transient absorption signals: (a) Ground-State Bleaching, (b) Stimulated Emission, and (c) Excited-State Absorption. Each pathway involves different transitions between the levels of a four-level system.

The integration of spectroscopic methods with imaging techniques, such as super-resolution microscopy and spectroscopic tomography, bridges the gap between molecular-level information and macroscopic observations [24]. Meanwhile, the application of artificial intelligence and machine learning approaches to spectral data analysis promises to reveal subtle patterns and correlations that might otherwise remain hidden.

As our understanding of light-matter interactions deepens and experimental capabilities advance, spectroscopy will continue to provide critical insights across chemistry, physics, biology, and materials science, contributing to technological innovations and fundamental scientific discoveries.

Bibliography

[1] Ángel Rivas et al. *Markovian Master Equations: A Critical Study* New Journal of Physics **12** p. 113032 (2010)

[2] Jannis Krumland et al. *Two-Dimensional Electronic Spectroscopy from First Principles.* Oct. 27, 2023. DOI: 10.48550/arXiv.2308.09062. arXiv: 2308.09062 [cond-mat]. URL: http://arxiv.org/abs/2308.09062. Pre-published.

[3] Javier Segarra-Martí et al. *Towards Accurate Simulation of Two-Dimensional Electronic Spectroscopy* Topics in Current Chemistry **376** p. 24 (2018)

[4] Haoran Sun et al. *Two-Dimensional Spectroscopy of Open Quantum Systems.* Dec. 14, 2024. DOI: 10.48550/arXiv.2412.10931. arXiv: 2412.10931 [cond-mat]. URL: http://arxiv.org/abs/2412.10931. Pre-published.

[5] Peter Hamm *Principles of Nonlinear Optical Spectroscopy: A Practical Approach* ()

[6] Shaul Mukamel. *Principles of Nonlinear Optical Spectroscopy.* New York: Oxford University Press, 1995. 543 pp. ISBN: 0-19-509278-3.

[7] Daniel Manzano *A Short Introduction to the Lindblad Master Equation* AIP Adv. **10** p. 025106 (2020)

[8] Heinz-Peter Breuer and Francesco Petruccione. *The Theory of Open Quantum Systems.* 1. publ. in paperback, [Nachdr.] Oxford: Clarendon Press, 2009. 613 pp. ISBN: 978-0-19-852063-4, 978-0-19-921390-0.

[9] Shaul Mukamel. *Principles of Nonlinear Optical Spectroscopy.* Oxford University Press, 1995.

[10] Robert W. Boyd. *Nonlinear Optics.* 3rd. Academic Press, 2008.

[11] Tameem Albash et al. *Quantum Adiabatic Markovian Master Equations* New Journal of Physics **14** p. 123016 (2012)

[12] Franklin D. Fuller and Jennifer P. Ogilvie *Experimental Implementations of Two-Dimensional Fourier Transform Electronic Spectroscopy* Annual Review of Physical Chemistry **66** pp. 667–690 (2015)

[13] Michael D. Fayer *Dynamics of Liquids, Molecules, and Proteins Measured with Ultrafast 2D IR Vibrational Echo Chemical Exchange Spectroscopy* Annual Review of Physical Chemistry **60** pp. 21–38 (2009)

[14] Minhaeng Cho. *Two-Dimensional Optical Spectroscopy.* CRC Press, 2009.

[15] Darius Abramavicius et al. *Coherent Multidimensional Optical Spectroscopy of Excitons in Molecular Aggregates; Quasiparticle versus Supermolecule Perspectives* Chemical Reviews **109** pp. 2350–2408 (2009)

[16] Shaul Mukamel *Multidimensional Femtosecond Correlation Spectroscopies of Electronic and Vibrational Excitations* Annual Review of Physical Chemistry **51** pp. 691–729 (2000)

[17] Y. Tanimura and R. Kubo *Time Evolution of a Quantum System in Contact with a Nearly Gaussian-Markoffian Noise Bath* Journal of the Physical Society of Japan **58** pp. 101–114 (1989)

[18] C. Scheurer and S. Mukamel *Design strategies for pulse sequences in multidimensional optical spectroscopies* Journal of Chemical Physics **115** pp. 4989–5004 (2001)

[19] David M. Jonas *Two-dimensional femtosecond spectroscopy* Annual Review of Physical Chemistry **54** pp. 425–463 (2003)

[20] Haiyan Tan and Shaul Mukamel *Coherent Multidimensional Optical Probes for Electronic and Vibrational Excitations: Principles and Applications* J. Chem. Phys. **129** p. 124505 (2008)

[21] Yuqing Yan and Shaul Mukamel *Phase Cycling Techniques in Multidimensional Optical Spectroscopy* J. Chem. Phys. **130** p. 234111 (2009)

[22] P. Tian et al. *Femtosecond Phase-Coherent Two-Dimensional Spectroscopy* Science **300** pp. 1553–1555 (2003)

[23] John D. Hybl et al. *Two-dimensional electronic spectroscopy* Chemical Physics Letters **297** pp. 307–313 (1998)

[24] Tobias Brixner et al. *Two-dimensional spectroscopy of electronic couplings in photosynthesis* Nature **434** pp. 625–628 (2005)

[25] Gabriela S. Schlau-Cohen, Akihito Ishizaki, and Graham R. Fleming *Two-dimensional electronic spectroscopy and photosynthesis: Fundamentals and applications to photosynthetic light-harvesting* Chemical Physics **386** pp. 1–22 (2011)

[26] Lionel Lepetit, Gilles Chériaux, and Manuel Joffre *Linear techniques of phase measurement by femtosecond spectral interferometry for applications in spectroscopy* Journal of the Optical Society of America B **12** pp. 2467–2474 (1995)

[27] Alan D. Bristow et al. *A versatile ultrastable platform for optical multidimensional Fourier-transform spectroscopy* Review of Scientific Instruments **80** p. 073108 (2009)

[28] Gregory S. Engel et al. *Evidence for wavelike energy transfer through quantum coherence in photosynthetic systems* Nature **446** pp. 782–786 (2007)

[29] Peter Hamm and Martin Zanni. *Concepts and Methods of 2D Infrared Spectroscopy.* Cambridge University Press, 2011.

[30] Munira Khalil, Nurettin Demirdöven, and Andrei Tokmakoff *Coherent 2D IR Spectroscopy: Molecular Structure and Dynamics in Solution* Journal of Physical Chemistry A **107** pp. 5258–5279 (2003)

[31] Sang-Hee Shim and Martin T. Zanni *How to turn your pump-probe instrument into a multidimensional spectrometer: 2D IR and Vis spectroscopies via pulse shaping* Physical Chemistry Chemical Physics **11** pp. 748–761 (2006)

[32] Rudi Berera, Rienk van Grondelle, and John T. M. Kennis *Ultrafast Transient Absorption Spectroscopy: Principles and Application to Photosynthetic Systems* Photosynthesis Research **101** pp. 105–118 (2009)

[33] Uwe Megerle et al. *Sub-50 fs broadband absorption spectroscopy with tunable excitation: putting the analysis of ultrafast molecular dynamics on solid ground* Applied Physics B **96** pp. 215–231 (2009)